Inorganic Chemistry

Article

pubs.acs.org/IC

# Octamolybdate-Based Metal–Organic Framework with Unsaturated Coordinated Metal Center As Electrocatalyst for Generating Hydrogen from Water

Yun Gong, Tao Wu, Peng Gang Jiang, Jian Hua Lin,* and Yong Xi Yang

Department of Applied Chemistry, College of Chemistry and Chemical Engineering, Chongqing University, Chongqing 400030, People's Republic of China

Supporting Information

**ABSTRACT:** Two octamolybdate-based MOFs with unsaturated coordinated metal centers formulated as $Cu_3(Mo_8O_{26})(H_2O)_2(OH)_2(L1)_4$ (L1 = 4*H*-4-amino-1,2,4-triazole) (**1**) and $Ag_4(Mo_8O_{26})(L2)_{2.5}(H_2O)$ (L2 = 3,5-dimethyl-4-amino-4*H*-1,2,4-triazole) (**2**) were synthesized and structurally characterized by single-crystal X-ray diffractions. Complex **1** exhibits a 1D chain-like structure. In complex **2**, 1D Ag-octamolybdate chains in the *ac* plane are covalently embedded into the 2D Ag-L2 layer, and the Ag-octamolybdate chains in the *bc* plane covalently link the 2D layers into 3D architecture. The two complexes both exhibit electrocatalytic activities toward generating $H_2$ from water with lowered overpotentials and enhanced currents, and the Cu complex exhibits better electrocatalytic activity toward generating $H_2$ from water than the Ag complex.

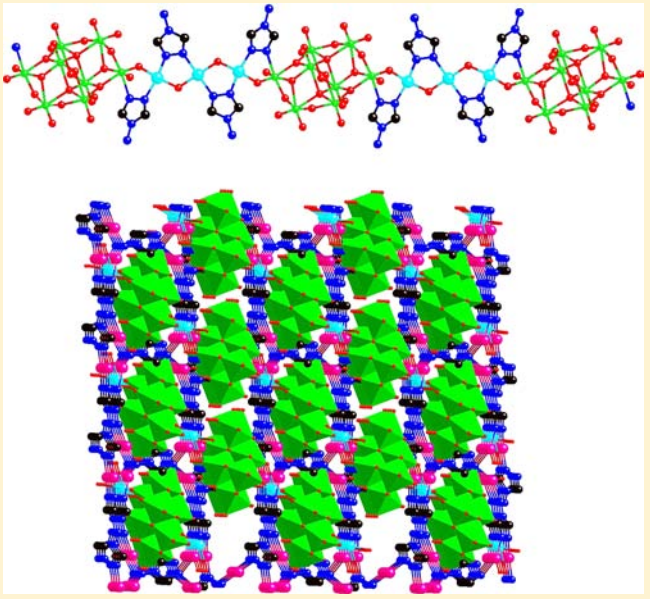

## INTRODUCTION

The molecular $H_2$ derived from noncarbon sources has emerged as a potential fuel for sustainable energy cycles that minimize carbon dioxide emissions.[1] The search for the catalysts that would allow facilitating the proton reduction to $H_2$ with use of cheap and earth-abundant metals is now an area of great interest.[2−4] Nature has evolved metal-dependent hydrogenase enzymes for producing $H_2$ from aqueous media with high efficiency and activity, but these molecules are usually instable under aerobic conditions. Many artificial enzyme catalysts for $H_2$ evolution have been developed, but most require the use of organic solvents, acids, additives, and fairly negative potentials. Thus the design of catalysts with high activity and stability in aqueous media at minimal overpotentials is a real challenge in this field.[5]

Polyoxometalates (POMs), a large family of soluble anionic metal oxide clusters of *d*-block transition metals (W, Mo, V), constitute ideal building blocks for targeting new functional materials[6] due to their wide range of redox and catalytic properties.[7] POM-based metal–organic framework (MOF) possesses insoluble framework, which attracts people's interest in heterogeneous catalysis. However, POM-based MOF has been rarely explored in the field of electrocatalyst for generating $H_2$ from water.[8]

Usually, the $H_2$ evolution reaction, $2H^+ + 2e^- = H_2$, involves a two-electron transfer mechanism. In the first step, a proton reacts with an electron to form a catalyst-bound hydrogen intermediate H* ($H^+ + e^- = H^*$). In the next step, either two H* recombine to form $H_2$, or another proton reacts with H* ($H^+ + H^* + e^- = H_2$). The best catalyst binds the intermediate neither too strongly nor too weakly.[9]

Based on the situation, in an attempt to obtain efficient electrocatalyst for generating $H_2$ from water, we utilize the octamolybdate-based MOF. The system is chosen based on the following considerations: (1) POM-based MOF is usually synthesized under acidic condition and it is not soluble in water. Thus it can be exposure to acidic aqueous solution for $H_2$ evolution reaction. (2) The element of Mo in octamolybdate possesses various chemical valences such as +4, +5, and +6, thus it displays superior redox property. (3) Octamolybdate cluster, as a usual isopolyoxometalate, has *α*-,

**Received:** August 29, 2012
**Published:** December 31, 2012

   dx.doi.org/10.1021/ic3018858 | *Inorg. Chem.* 2013, 52, 777−784

$\beta$-, $\gamma$-, $\delta$-, and $\varepsilon$-forms.[10] The five isomers can be interconverted, thus reversible interconversion for the cluster is possible during the electrocatalysis process. (4) It is expected that octamolybdate-based MOF can act as a bifunctional catalyst if unsaturated coordinated metal(II) center is included, which may provide an active center for H* binding.

In the present work, two octamolybdate-based MOFs formulated as $Cu_3(Mo_8O_{26})(H_2O)_2(OH)_2(L1)_4$ (L1 = 4*H*-4-amino-1,2,4-triazole) (**1**) and $Ag_4(Mo_8O_{26})(L2)_{2.5}(H_2O)$ (L2 =3,5-dimethyl-4-amino-4*H*-1,2,4-triazole) (**2**) are obtained via hydrothermal technique in moderate yields (Scheme 1). Their

**Scheme 1. Schematic Representations of L1 (a) and L2 (b)**

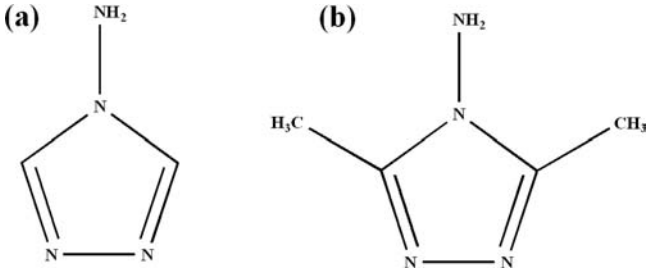


cyclic voltammograms (CVs), electrochemical impedance spectroscopies (EISs), controlled potential electrolysis (CPE) experiments, thermal stabilities, and UV−vis absorption spectra have been investigated.

## EXPERIMENTAL SECTION

**General Considerations.** All chemicals purchased were of reagent grade and used without further purification. C, H, and N elemental analyses were performed on an Elementar Vario MICRO E III analyzer. IR spectra were recorded as KBr pellets on a PerkinElmer spectrometer. The powder XRD (PXRD) data were collected on a RIGAKU DMAX2500PC diffractometer, using Cu K$\alpha$ radiation. Thermogravimetric analysis (TGA) and simultaneous differential scanning calorimetry (DSC) were performed on a NETZSCH5 STA 449C thermogravimetric analyzer in flowing Ar with a heating rate of 10 °C·min$^{-1}$. UV−vis spectra were measured on a HITACHI U-4100 UV−vis spectrophotometer. A Shiruisi RST5200 electrochemical analyzer was used in the electrochemical measurements. The gas sample composition was analyzed with a Varian GC-3800 gas chromatograph with a Molecular Sieve 5 Å column (40 m), where 5 mL of methane was injected as an internal standard.

**Electrochemical Measurements.** Acetone dispersion of samples (0.1 mL) and 0.01 mL of nafion solution were deposited on a glassy carbon electrode to obtain the working electrodes after the solvent is dried by an IR lamp. An Ag/AgCl electrode and a platinum foil were used as the reference and counter electrodes, respectively. For the electrocatalysis of $H_2$ production from water, the cyclic voltammgrams were recorded in 20 mL of $N_2$ degassed solution. Both positive and negative CV scans were performed on each sample. The mass of samples on the working electrode was $4.0 \times 10^{-1}$ mg. The mass of ligand in the solution was $4.0 \times 10^{-1}$ mg. Electrochemical impedance spectroscopy (EIS) measurements were carried out with a sinusoidal signal of 10 mV amplitude over the frequency range from 1 Hz to 1 MHz.

**Synthesis of $Cu_3(Mo_8O_{26})(H_2O)_2(OH)_2(L1)_4$ (1).** A mixture of L1 (0.1 mmol, 0.084 g), $Na_2MoO_4{\cdot}2H_2O$ (0.1 mmol, 0.24 g), $CuCl_2{\cdot}2H_2O$ (0.1 mmol, 0.17 g), and water (8 mL) was adjusted to pH 1.0 by $HNO_3$, and then heated at 160 °C in Teflon-lined autoclaves for 3 days, followed by slow cooling to room temperature. The resulting blue block crystals were filtered off (yield: ca. 32% based on Mo). Elemental Anal. Found: C, 5.37; H, 1.29; N, 12.62. Calcd for $C_8H_{22}Cu_3Mo_8N_{16}O_{30}$: C, 5.40; H, 1.25; N, 12.59. IR (KBr, cm$^{-1}$): 3499 (m), 3291 (m), 3207 (w), 3143 (w), 3105 (m), 2351 (w), 2286 (w), 1635 (m), 1612 (w), 1549 (w), 1392 (w), 1344 (w), 1277 (w), 1232 (w), 1085 (w), 1065 (w), 1044 (w), 983 (w), 960 (m), 927 (w), 911 (m), 856 (m), 766 (w), 694 (m), 659 (m), 627 (m), 58 5(w), 558 (w), 529 (w), 487 (w), 442 (w).

**Synthesis of $Ag_4(Mo_8O_{26})(L2)_{2.5}(H_2O)$ (2).** A mixture of L2 (0.1 mmol, 0.011 g), $MoO_3$ (0.11 mmol, 0.16 g), $AgNO_3$ (0.04 mmol, 0.007 g), and water (8 mL) was adjusted to pH 1.0 by $HNO_3$, and then heated at 170 °C in Teflon-lined autoclaves for 3 days, followed by slow cooling to room temperature. The resulting colorless block crystals were filtered off (yield: ca. 40% based on Mo). Elemental Anal. Found: C, 6.30; H, 1.15; N, 7.33. Calcd for $C_{10}H_{22}Ag_4Mo_8N_{10}O_{27}$: C, 6.28; H, 1.16; N, 7.32. IR (KBr, cm$^{-1}$): 3476 (s), 3335 (m), 2925 (w), 2361 (w), 1619 (m), 1555 (m), 1427 (w), 1375 (w), 1271 (w), 901 (s), 849 (w), 708 (m), 656 (w), 580 (w), 512 (w).

**X-ray Crystallography.** Single-crystal X-ray data for complexes **1** and **2** were collected on a Bruker-APEX CCD area detector-equipped diffractometer, using graphite monochromated Mo Ka ($\lambda$ = 0.71073 Å) radiation at room temperature. Empirical absorption correction was applied. The structures were solved by direct methods and refined by the full-matrix least-squares methods on $F^2$, using the SHELXTL-97 software.[11] All non-hydrogen atoms were refined anisotropically. All of the hydrogen atoms were placed in the calculated positions. The crystal data and structure refinements for complexes **1** and **2** are summarized in Table 1. Selected bond lengths and angles for complexes **1** and **2** are listed in Table 2. The CCDC reference numbers are the following: 879774 for complex **1** and 879775 for complex **2**.

**Table 1. Crystal Data and Structure Refinements for Complexes 1 and 2[a]**

| | 1 | 2 |
|---|---|---|
| empirical formula | $C_8H_{22}Cu_3Mo_8N_{16}O_{30}$ | $C_{10}H_{22}Ag_4Mo_8N_{10}O_{27}$ |
| $M$ | 1780.56 | 1913.38 |
| crystal system | triclinic | triclinic |
| space group | $P\bar{1}$ | $P\bar{1}$ |
| $a$/Å | 8.9318(8) | 11.0715(1) |
| $b$/Å | 11.1272(9) | 12.3855(1) |
| $c$/Å | 11.2538(1) | 14.7951(2) |
| $\alpha$/deg | 116.636(2) | 75.6310(1) |
| $\beta$/deg | 100.8770(1) | 82.335(2) |
| $\gamma$/deg | 94.3770(1) | 69.8860(1) |
| $V$/Å$^3$ | 965.17(1) | 1842.9(3) |
| $Z$ | 1 | 2 |
| $D_{calcd}$/g cm$^{-3}$ | 3.063 | 3.448 |
| $\mu$/mm$^{-1}$ | 4.241 | 4.801 |
| no. of unique reflcns | 3331 | 6287 |
| reflcns used [$I > 2\sigma(I)$] | 2929 | 4544 |
| $F$(000) | 845 | 1784 |
| goodness-of-fit on $F^2$ | 1.080 | 1.043 |
| final $R$ indices [$I > 2\sigma(I)$] | $R_1$ = 0.0284 | $R_1$ = 0.0703 |
| | $wR_2$ = 0.0703 | $wR_2$ = 0.1945 |

[a] $R_1 = \sum||F_o| - |F_c||/\sum|F_o|$; $wR_2 = \sum[w(F_o^2 - F_c^2)^2]/\sum[w(F_o^2)^2]^{1/2}$.

## RESULTS AND DISCUSSION

**Crystal Structure of $Cu_3(Mo_8O_{26})(H_2O)_2(OH)_2(L1)_4$ (1).** Single-crystal X-ray diffraction analysis reveals that complex **1** crystallizes in the *triclinic* space group $P\bar{1}$ (Table 1). In complex **1**, the asymmetric unit contains two Cu(II), two L1, half $[Mo_8O_{26}]^{4-}$, one $\mu_2$-OH and one coordinated water molecule. The crystallographically independent Cu(1) exhibits a slightly distorted square-planar unsaturated coordination geometry, defined by two nitrogen atoms from two L1, one oxygen atom from $\mu_2$-OH, and one terminal oxygen atom from $[Mo_8O_{26}]^{4-}$


dx.doi.org/10.1021/ic3018858 | Inorg. Chem. 2013, 52, 777−784

**Table 2. Selected Bond Lengths (Å) and Angles (deg) for Complexes 1 and 2**[a]

| | | | |
|---|---|---|---|
| Complex **1** | | | |
| Cu(1)−O(14) | 1.885(3) | Cu(1)−O(9) | 1.926(4) |
| Cu(1)−N(5) | 1.956(4) | Cu(1)−N(2) | 1.993(4) |
| Cu(2)−O(14) | 1.911(4) | Cu(2)−O(15) | 2.631(5) |
| Cu(2)−N(6) | 2.040(4) | Mo(3)−N(1) | 2.318(4) |
| N(5)−Cu(1)−N(2) | 165.93(2) | O(14)−Cu(2)−O(15) | 85.64(2) |
| O(14)−Cu(1)−O(9) | 166.68(2) | O(14)#1−Cu(2)−O(14) | 180.00 |
| N(6)−Cu(2)−O(15) | 79.06(2) | N(6)#1−Cu(2)−O(15) | 100.94(2) |
| Complex **2** | | | |
| Ag(1)−O(3) | 2.369(1) | Ag(1)−O(20) | 2.581(1) |
| Ag(2)−N(2) | 2.151(1) | Ag(3)−N(5) | 2.132(2) |
| Ag(3)−N(1) | 2.137(1) | Ag(4A)−O(13) | 2.439(2) |
| Ag(4A)−N(12) | 2.32(3) | Ag(4B)−N(6) | 2.124(2) |
| Ag(5A)−N(10) | 2.17(3) | Ag(5B)−N(10) | 2.10(3) |
| Ag(5B)−O(27) | 2.02(3) | Ag(5A)−O(27) | 2.440(2) |
| O(17)−Ag(1)−O(20) | 73.6(4) | O(3)−Ag(1)−O(17) | 164.2(5) |
| O(3)−Ag(1)−O(20) | 121.6(4) | N(2)#2−Ag(2)−N(2) | 180 |
| N(5)−Ag(3)−N(1) | 164.8(6) | N(6)−Ag(4A)−N(12) | 142.9(1) |
| N(10)−Ag(5A)−O(27) | 115.1(1) | N(10)−Ag(5A)−N(8)#3 | 149.7(1) |

[a]Symmetry transformations used to generate equivalent atoms: #1 $-x+1, -y, -z$; #2 $-x+1, -y+2, -z$; #3 $-x+2, -y+1, -z+1$.

[Cu−O 1.885(3)−1.926(4) Å, Cu−N 1.956(4)−1.993(4) Å] (Table 2). Cu(2) sits on the inversion center and shows a slightly distorted octahedral coordination geometry, supplied by two nitrogen atoms from two L1, two oxygen atoms from two $\mu_2$-OH in the equatorial positions [Cu−O 1.911(4) Å, Cu−N 2.040(4) Å] and two oxygen atoms from two aqua ligands in the apical position with a 2.631(5) Å of Cu−O distance, which is a bit longer than the normal Cu−O bond length, indicating the binding of the water molecule is weak (Table 2). In complex **1**, the two crystallographically independent L1 ligands both act as $\mu_2$-bridges. One links two Cu(II) centers via two nitrogen atoms with a Cu···Cu separation of 3.352 Å, and another connects the Cu(II) and Mo(VI) centers with a Cu···Mo separation of 3.451 Å [Mo−N 2.318(4) Å] (Table 2), leaving the $NH_2$ group uncoordinated (Figure 1a). The $[Mo_8O_{26}]^{4-}$ moiety has $C_i$ symmetry and is composed of six edge-sharing $\{MoO_6\}$ octahedra and two $\{MoO_5N\}$ octahedra and thus displays the characteristic $\gamma$-octamolybdate arrangement (Figure 1b).[10a] In complex **1**, Cu(II) ions are linked by $\mu_2$-L1 and $\mu_2$-OH into a $Cu_3$ unit, which is further connected by $[Mo_8O_{26}]^{4-}$ to give a one-dimensional (1D) chain (Figure 1).

**The Electrocatalytic Activity of Complex 1.** The phase purities of complexes **1** and **2** were supported by the powder X-ray diffraction (PXRD) patterns of the bulk samples, which are consistent with the calculated patterns (Figure S1). The electrocatalytic activity of complex **1** toward generating $H_2$ from water was evaluated by cyclic voltammograms (CVs) in $H_2SO_4$ aqueous solution. For comparison, the electrochemical

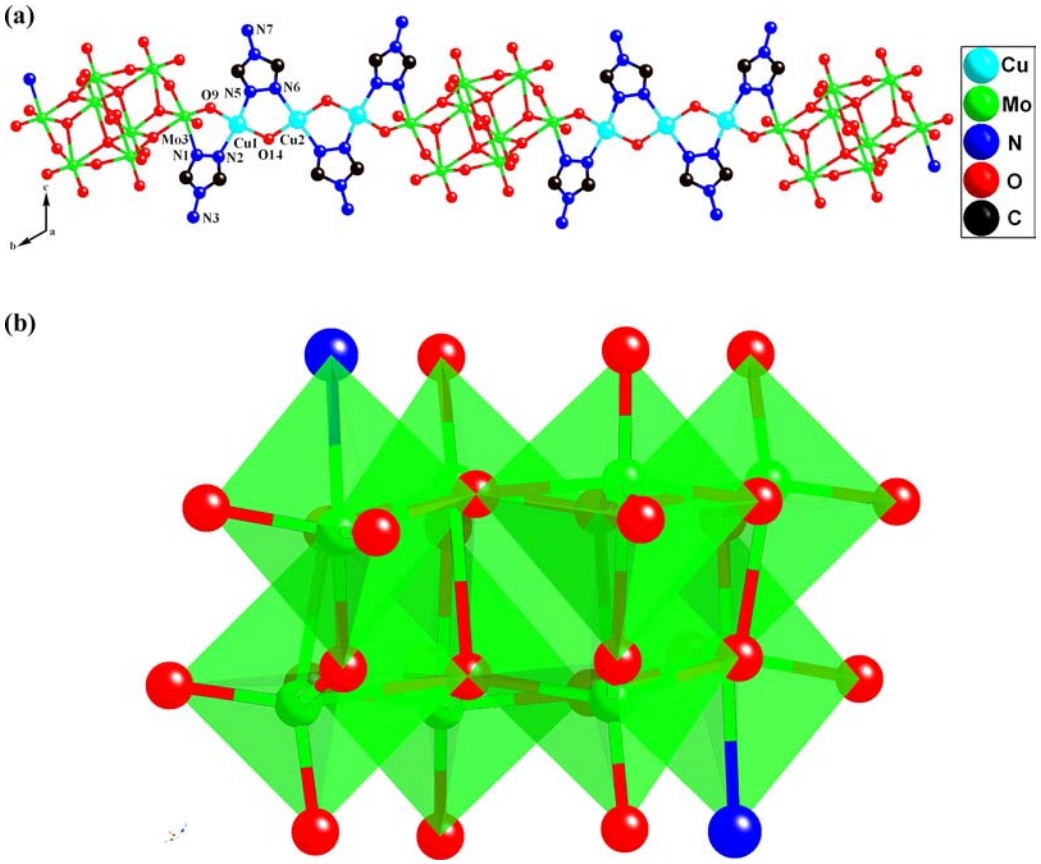


**Figure 1.** 1D chain constructed by $Cu_3$ unit and $[Mo_8O_{26}]^{4-}$ in complex **1** (H atoms and water molecules omitted for clarity) (a); polyhedral representation of the $\gamma$-$[Mo_8O_{26}]^{4-}$ moiety in complex **1** (b).


dx.doi.org/10.1021/ic3018858 | *Inorg. Chem.* 2013, 52, 777−784

behavior at the bare carbon glassy electrode (GCE) was also studied. Figure 2 shows the CVs in 0.5 M $H_2SO_4$ aqueous solution in the potential range from −1.2 to 1.8 V vs Ag/AgCl at 50 mV·s$^{-1}$. As we know, in 0.5 M $H_2SO_4$ aqueous solution, the potential for $H_2$ evolution reaction (HER) on a clean Pt electrode is −0.24 V vs Ag/AgCl, indicating the overpotential range in Figure 2 is −0.96−2.04 V. An irreversible peak at −0.82 V vs Ag/AgCl (overpotential $\eta$ = −0.58 V) was observed at the bare GCE (Figure 2), which coincides with the evolution of bubbles, corresponding to the generation of $H_2$ from water. When the 0.5 M $H_2SO_4$ aqueous solution contains L1, the irreversible peak at the bare GCE was shifted to more negative potential ($\eta$ = −0.62 V) and the peak current decreases (Figure 2), indicating the free ligand L1 cannot catalyze HER. It is expected that L1 might not act as an electron-transfer promoter under the condition.[12] When the **1**-modified electrode (**1**-GCE) was utilized, the reduction peak of $H^+$ in 0.5 M $H_2SO_4$ aqueous solution is obviously shifted to more positive potential ($\eta$ = −0.43 V) accompanied by the enhanced current, suggesting complex **1** has good electrocatalytic activity for HER (Figure 2).[13] Complex **1** can lower the overpotential of HER, which is also evidenced by the Tafel curve at **1**-GCE in $H_2SO_4$ aqueous solution (Figure S2). The quasireversible redox couple with a half-wave overpotential of 0.72 V ($E_{pa}$ = 0.82 V and $E_{pc}$= 0.62 V, $E_{pa}$ = anodic peak overpotential, $E_{pc}$ =

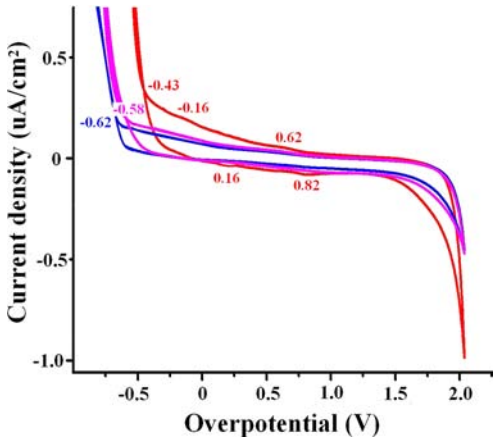


**Figure 2.** Cyclic voltammograms of the bare GCE (pink) and **1**-GCE (red) in 0.5 M $H_2SO_4$ aqueous solution at a sweep rate of 50 mV·s$^{-1}$. The blue curve indicates the CV of the bare GCE in the similar solution containing 0.4 mg of L1.

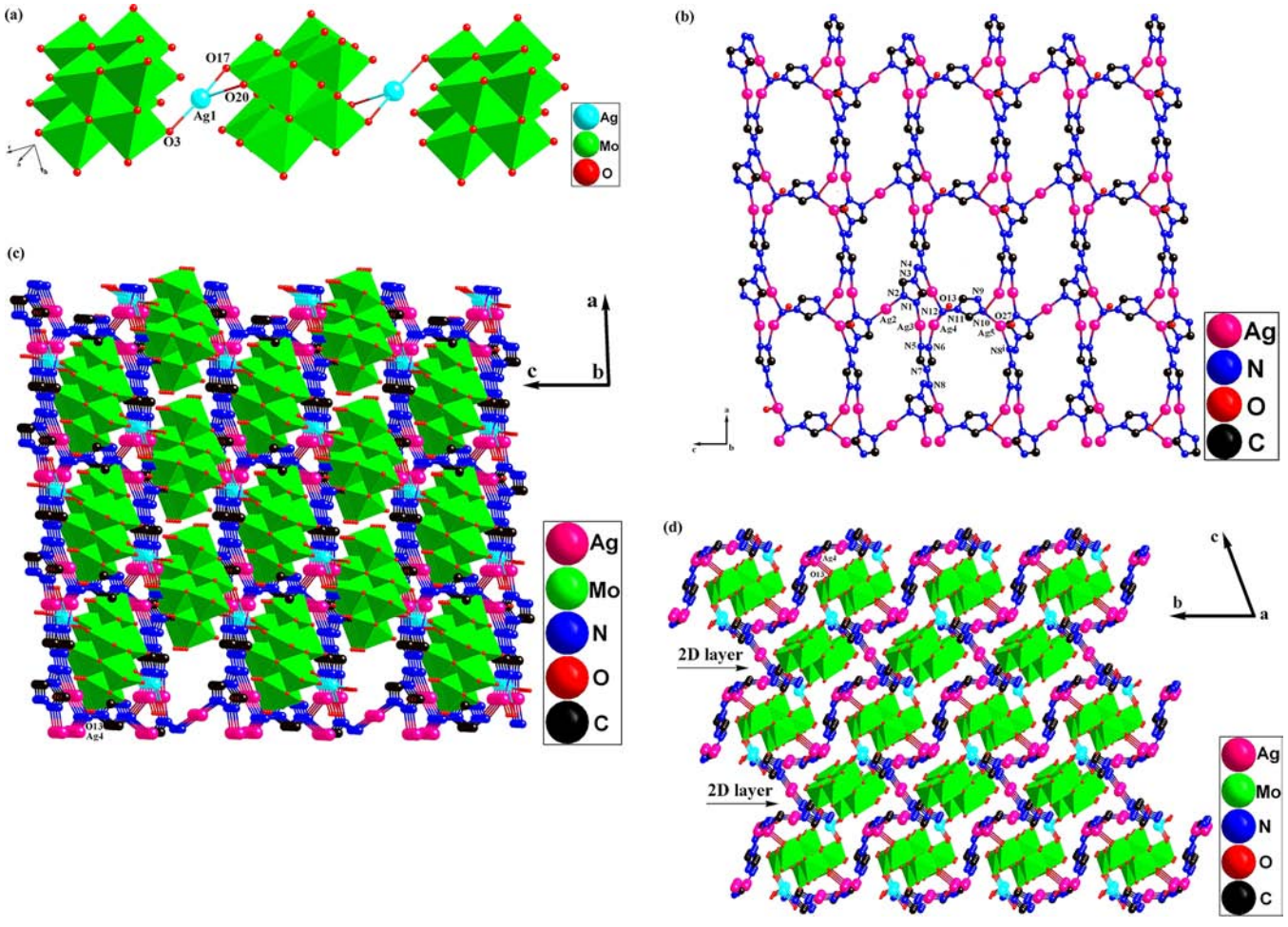


**Figure 3.** 1D inorganic chain consisting of Ag(I) and $\beta$-$[Mo_8O_{26}]^{4-}$ in complex **2** (H atoms and L2 omitted for clarity) (a); 2D MOF layer built from Ag(I) and L2 (atom with additional superscript i refers to the symmetry operation: $-x + 2$, $-y + 1$, $-z + 1$, H atoms and methyl groups of L2 omitted for clarity) (b); 1D inorganic chains in the *ac* plane embedded into 2D MOF layer via Ag−O linkage (c); 2D layers connected by 1D inorganic chains in the *bc* plane into 3D architecture (d) (Ag from 1D chains denoted in sapphire, H atoms and methyl groups of **L2** omitted for clarity).


dx.doi.org/10.1021/ic3018858 | *Inorg. Chem.* 2013, 52, 777−784

cathodic peak overpotential) at the **1**-GCE may be assigned to the Cu-based oxidation of complex **1** (Figure 2).[14] The redox of the $[Mo_8O_{26}]^{4-}$ polyanion is overlapped by the potential for HER with peaks at −0.16 and 0.16 V in the system (Figure 2).[8a,15]

In the presence of complex **1**, the electrocatalytic current grows larger with increasing acid concentrations, as shown in Figure S3. The peak currents were also proportional to the scan rates (Figure S4), indicating that the redox process is diffusion-controlled,[13] and the exchanging rate of electrons is fast. The result is also in agreement with the electrochemical impedance spectroscopy (EIS). As shown in Figure S5, the Nyquist plots of **1**-GCE and the bare GCE are similar, in which a sloped line is observed. The slope of the impedance curve in the low-frequency region for **1**-GCE is higher than that for the bare GCE, implying the resistance for complex **1** is higher than that for the bare electrode.[16] When **1**-GCE is utilized, with the increase of the electrode resistance, the overall impedance of the three-electrode cell is more than that of the blank system. Usually, current decreases with the increase of impedance. The abnormal enhanced current of HER at **1**-GCE indicates the additional reduction current is related to the structure of complex **1**, and it probably originates from the redox of $[Mo_8O_{26}]^{4-}$ moiety in the framework, which is overlapped by the potential for HER.

Controlled potential electrolysis (CPE) experiments at −0.8 V vs AgCl/Ag ($\eta$ = −0.56 V and current density =0.7 uA/cm$^2$) were also performed to provide evidence for catalytic activity of complex **1**. As depicted in Figure S6, **1**-GCE affords a robust and essentially linear charge build-up over time, with no substantial loss in activity over the course of 2 h, which shows higher charge build-up than the bare GCE under the same condition ($\eta$ = −0.56 V and current density = 0.1 uA/cm$^2$) (Figure S6). Moreover, **1**-GCE is stable. When the potential range is maintained at −1.0 to 2.0 V vs AgCl/Ag, the peak currents can be kept over one hundred cycles. The behavior at **1**-GCE is indicative of the possible reversible structural transformation between the oxidization and reduction states of the species during the redox process.

To estimate the Faradaic efficiency for $H_2$ production by complex **1**, the evolved $H_2$ in the 2 h CPE experiment is characterized and proved by gas chromatography. The generated $H_2$ volume matches that calculated based on the amount of charge consumed, indicating the catalyst operates at 98% Faradaic efficiency (see the Supporting Information). On the basis of the amount of complex **1** used in the experiment, a turnover number (TON) of $2.6 \times 10^3$ mol of $H_2$ per mole of catalyst is calculated.

**Crystal Structure of $Ag_4(Mo_8O_{26})(L2)_{2.5}(H_2O)$ (2).** To further investigate the relationship between the electrocatalytic activity and the structure of the octamolybdate-based MOF, we got another complex, $Ag_4(Mo_8O_{26})(L2)_{2.5}(H_2O)$ (**2**).

Complex **2** crystallizes in the *triclinic* space group $P\bar{1}$ (Table 1), it contains three and two half Ag(I), two and a half L2, and two half $[Mo_8O_{26}]^{4-}$, and one coordinated water molecule in the asymmetric unit. Due to the disorder, the occupancy factor of one L2 ligand is 0.5, which is constructed by N9−N12 and C9−C12, the second site of each atom from the L2 ligand is calculated from the first position of the atom via the inversion operation. Ag(1) adopts a slightly distorted planar triangular coordination geometry, defined by three terminal oxygen atoms from two $[Mo_8O_{26}]^{4-}$[Ag−O 2.369(1)− 2.581(1) Å] (Figure 3a and Table 2). Ag(2) sits on the inversion center and it is unsaturated coordinated by two triazol nitrogen atoms from two L2 to give a linear geometry, and Ag(3) also exhibits a similar unsaturated coordination environment [Ag−N 2.132(2)−2.151(1) Å] (Figure 3b,c). Ag(4) is disordered over two locations and the occupancy factors of Ag4A and Ag4B are 0.45 and 0.55, respectively. Ag(4) is three coordinated by two nitrogen atoms from two L2 and one terminal oxygen atom from $[Mo_8O_{26}]^{4-}$ to furnish a distorted planar triangular coordination environment [Ag−N 2.124(2)−2.32(3) Å, Ag−O 2.439(2) Å] (Figure 3b,c). Ag(5) is disordered over two locations, and the occupancy factors of Ag5A and Ag5B are 0.35 and 0.15, respectively. Ag(5) shows a distorted planar triangular geometry, supplied by two nitrogen atoms from two L2 and one oxygen atom from the water molecule [Ag−N 2.10(3)−2.17(3) Å, Ag−O 2.02(3)−2.440(2) Å] (Figure 3b,c). The $[Mo_8O_{26}]^{4-}$ moiety in complex **2** possesses $C_{2h}$ symmetry and has eight edge-sharing $\{MoO_6\}$ octahedra, indicating the $[Mo_8O_{26}]^{4-}$ moiety displays the characteristic $\beta$-octamolybdate arrangement. Different $\beta$-$[Mo_8O_{26}]^{4-}$ are linked by Ag(I) via terminal oxygen atoms into the 1D chain along different directions (Figure 3a). In complex **2**, different Ag(I) ions are connected by L2 into the two-dimensional (2D) MOF layer (Figure 3b). Ag-octamolybdate chains in the *ac* plane are covalently embedded into the 2D MOF layer via Ag−O linkage (Ag4−O13 2.439(16) Å) (Figure 3c). Ag-octamolybdate chains in the *bc* plane connect the 2D layers via similar Ag−O linkage into three-dimensional (3D) architecture (Figure 3d).

**The Electrocatalytic Activity of Complex 2.** As for complex **2**, its electrocatalytic activity toward generating $H_2$ from water was also evaluated under similar condition. The CV reveals the reduction overpotential of $H^+$ is shifted to −0.49 V accompanied by the enhanced current at the **2**-modified electrode (**2**-GCE), indicating complex **2** also can catalyze the generation of $H_2$ from water (Figure 4). Complex **2** can lower the overpotential of HER, which is also evidenced by the Tafel curve at **2**-GCE in $H_2SO_4$ aqueous solution (Figure S2). Whereas for the free ligand L2, the irreversible peak was observed at more negative potential ($\eta$ = −0.65 V) and the peak current decreases (Figure 4), indicating the free ligand L2 cannot catalyze HER. In the presence of complex **2**, the

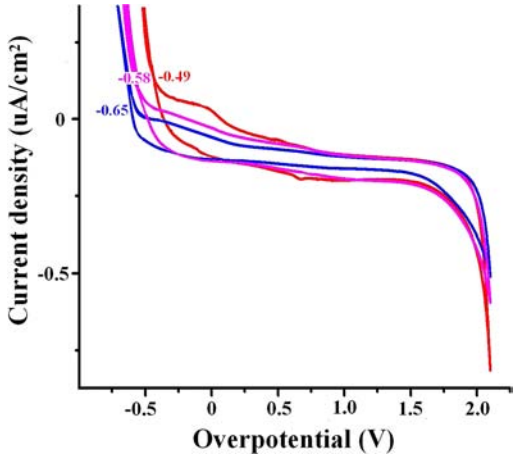


**Figure 4.** Cyclic voltammograms of the bare GCE (pink) and **2**-GCE (red) in 0.5 M $H_2SO_4$ aqueous solution at a sweep rate of 50 mV·s$^{-1}$. The blue curve indicates the CV of the bare GCE in the similar solution containing 0.4 mg of L2.


dx.doi.org/10.1021/ic3018858 | *Inorg. Chem.* 2013, 52, 777−784

electrocatalytic current grows larger with increasing acid concentrations, as shown in Figure S7. And the peak currents were also proportional to the scan rates (Figure S8). EIS measurement shows the redox process is diffusion-controlled and the impedance of the half cell in the presence of **2**-GCE is more than that for the bare-GCE, indicating the electrode resistance of **2**-GCE is more than that of the bare-GCE (Figure S5). The abnormal enhanced current for HER at **2**-GCE is related to the framework of complex **2**. The catalytic activity of complex **2** is also evidenced by the CPE experiment ($\eta$ = −0.56 V and current density = 0.3 uA/cm$^2$), in which **2**-GCE shows higher charge build-up than the bare GCE under the same condition ($\eta$ = −0.56 V and current density = 0.1 uA/cm$^2$) (Figure S9) with the Faradaic efficiency of 97% and TON of $3.0 \times 10^2$ mol of $H_2$ per mole of complex **2**.

Comparing complexes **1** and **2**, the reduction overpotential of $H^+$ at **1**-GCE (−0.43 V) is more positive than that at **2**-GCE (−0.49 V) (Figure S10), indicating the Cu complex **1** possesses better catalytic activity than the Ag complex **2**. The result is in agreement with the 2 h-CPE experiment, in which **1**-GCE shows higher charge build-up than **2**-GCE under the same condition (Figure S11). Because the lowered overpotential is related to the active center of electrocatalyst for H* binding,[9] complex **1** reduces the overpotential of $H_2$ evolution greater than complex **2**, as shown by the Tafel curves in Figure S2, which is probably due to their different unsaturated coordinated metal centers in the structures.[9] The detailed mechanism is under investigation. The present work shows it is possible to obtain better electrocatalyst with the cheaper metal ion by the rational design and synthesis of POM-based MOFs.

**Thermal Stability of Complexes 1 and 2.** To examine the thermal stability of complexes **1** and **2**, TGA and simultaneous DSC were carried out. The samples were heated to 650 °C in Ar. As the black curve shows in Figure 5a, complex **1** exhibits one step of weight loss in the range of 150−260 °C with a loss of 2.0 wt % (calcd 1.9 wt %), corresponding to the loss of coordinated water. In the similar range, the DSC plot of complex **1** shows a broad endotherm with a peak at 200 °C. When the temperature is in the range of 410−500 °C, complex **1** exhibits one step of weight gain, and the calorimetric curve shows an endotherm with a peak at 415 °C, which might correspond to the phase change of the molybdenum oxide.

As for complex **2**, it releases its coordinated water in the range of 150−260 °C (calcd 0.9%; obsd 1.0%), as the black curve shows in Figure 5b. In the similar range, the DSC curve of complex **2** shows an endotherm with a peak at 170 °C. The pyrolysis of organic ligand exhibits two endothermal peaks at 280 and 343 °C, respectively (Figure 5b). Similar to complex **1**, complex **2** shows one step of weight gain in the range of 440−510 °C, and the calorimetric curve shows two endothermal peaks at 442 and 473 °C, respectively, probably corresponding to the phase change of the molybdenum oxide.

**UV−vis Absorption Spectra of Complexes 1 and 2.** The UV−vis absorption spectra of complexes **1** and **2** together with the free organic ligands in the solid state at room temperature are shown in Figure 6. As shown in Figure 6, L1 and L2 exhibit strong absorption with maxima at 294 and 288 nm in the range of 250−400 nm, respectively, which probably corresponds to the $\pi-\pi^*$ transition of the triazol ring.[17,18] As we know, the electron-withdrawing substituent of a ligand will lower the energy of the $\pi-\pi^*$ transition and lead to the bathocromic effect of the absorption band.[18] The absorption maximum of L2 (288 nm) is blue-shifted 6 nm compared to

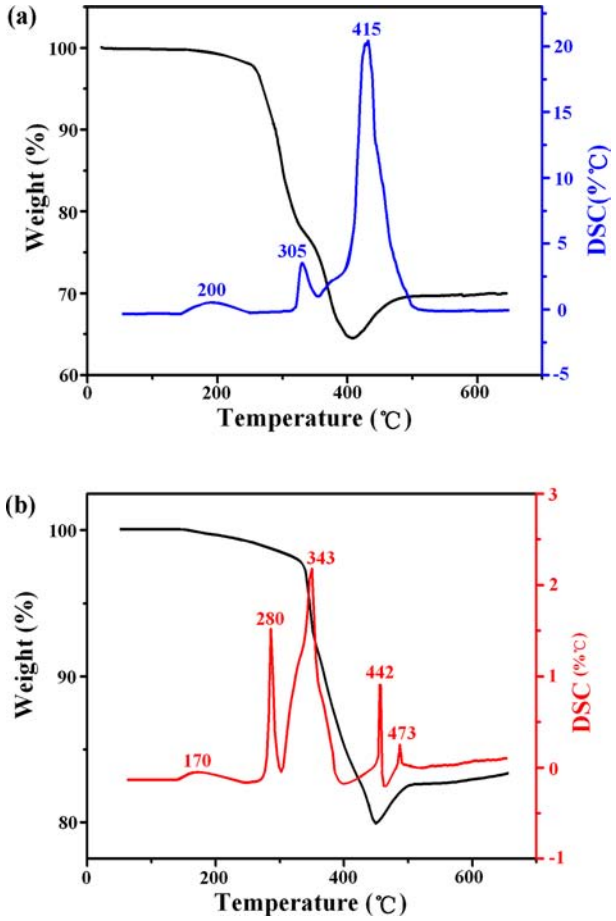


**Figure 5.** TG and DSC curves for complexes **1** (a) and **2** (b).

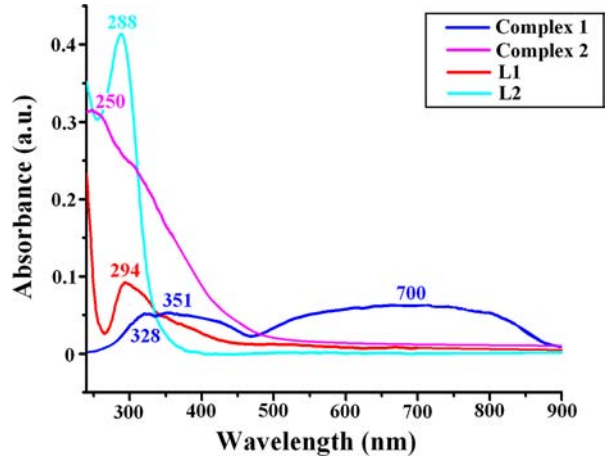


**Figure 6.** UV−vis absorption spectra at room temperature for the free ligands L1 and L2 and complexes **1** and **2**.

that of L1 (294 nm), which is the result of the methyl substituent (electron-donoring group) in the structure of L2.

As for complex **1**, it displays absorption in the range of 240−400 nm with maxima at 328 and 351 nm. As for complex **2**, it exhibits strong absorption with maxima at 250 nm in the range of 240−400 nm, which are different from those of free ligands, inferring that the absorption of complexes **1** and **2** may be associated with the Mo−O LCMT bands.[19] The broad absorption band of complex **1** in the range 460−900 nm corresponds to the visible d--d transition.


dx.doi.org/10.1021/ic3018858 | *Inorg. Chem.* 2013, 52, 777−784

## CONCLUSIONS

In conclusion, based on $[Mo_8O_{26}]^{4-}$, two MOFs formulated as $Cu_3(Mo_8O_{26})(H_2O)_2$ $(OH)_2(L1)_4$ (**1**) and $Ag_4(Mo_8O_{26})$-$(L2)_{2.5}(H_2O)$ (**2**) have been synthesized. The two MOFs are stable and not soluble in acidic aqueous solution. Complex **1** exhibits a 1D chain-like structure. In complex **2**, 1D Ag-octamolybdate chains in the *ac* plane are covalently embedded into 2D Ag-L2 layer, and the Ag-octamolybdate chains in the *bc* plane covalently link the 2D layers into 3D architecture. The two complexes both exhibit electrocatalytic activity toward generating $H_2$ from water with lowered overpotentials and enhanced currents. Complex **1** reduces the overpotential of HER greater than complex **2**, which is probably related to their different unsaturated coordinated metal centers in the structures. It is expected that the enhanced current for HER probably originates from the redox of the $[Mo_8O_{26}]^{4-}$ polyanion overlapped by the potential of the proton reduction. The detailed mechanism is under investigation. The present work shows it is possible to obtain better electrocatalyst by using the cheaper metal ion instead of noble metal ion.

## ASSOCIATED CONTENT

### Supporting Information

Crystallographic data and additional material mentioned in the text. This material is available free of charge via the Internet at http://pubs.acs.org. Copies of X-ray crystallographic files in CIF format for the structure determination may be obtained free of charge from The Director, CCDC, 12 Union Road, Cambridge, CB2 IEZ, UK (Fax: +44−1223−336033; e-mail: deposit@ccdc.cam.ac.uk).

## AUTHOR INFORMATION

### Corresponding Author

*Tel.: +86-023-65102316. E-mail: jhlin@cqu.edu.cn or jhlin@pku.edu.cn.

### Notes

The authors declare no competing financial interest.

## ACKNOWLEDGMENTS

Financial support from the Natural Science Foundation Project of Chongqing (No. CSTC 2011jjA50017) is gratefully acknowledged.

## REFERENCES

(1) (a) Turner, J. A. *Science* **2004**, *305*, 972. (b) Lewis, N. S.; Nocera, D. G. *Proc. Natl. Acad. Sci. U.S.A.* **2006**, *103*, 15729.

(2) (a) Sun, Y. J.; Bigi, J. L. P.; Piro, N. A.; Tang, M. L.; Long, J. R.; Chang, C. J. *J. Am. Chem. Soc.* **2011**, *133*, 9212. (b) Voloshin, Y. Z.; Dolganov, A. V.; Varzatskii, O. A.; Bubnov, Y. N. *Chem. Commun.* **2011**, *47*, 7737. (c) Artero, V.; Chavarot-Kerlidou, M.; Fontecave, M. *Angew. Chem., Int. Ed.* **2011**, *50*, 7238. (d) Esswein, A. J.; Nocera, D. G. *Chem. Rev.* **2007**, *107*, 4022. (e) DuBois, M. R.; DuBois, D. L. *Chem. Soc. Rev.* **2009**, *38*, 62. (f) Gloaguen, F.; Rauchfuss, T. B. *Chem. Soc. Rev.* **2009**, *38*, 100.

(3) (a) Frey, M. *ChemBioChem* **2002**, *3*, 153. (b) Fontecilla-Camps, J. C.; Volbeda, A.; Cavazza, C.; Nicolet, Y. *Chem. Rev.* **2007**, *107*, 4273. (c) Merki, D.; Fierro, S.; Vrubel, H.; Hu., X. L. *Chem. Sci.* **2011**, *2*, 1262. (d) Merki, D.; Vrubel, H.; Rovelli, L.; Fierro, S.; Hu, X. L. *Chem. Sci.* **2012**, *3*, 2515.

(4) (a) Darensbourg, M. Y.; Lyon, E. J.; Zhao, X.; Georgakaki, I. P. *Proc. Natl. Acad. Sci. U.S.A.* **2003**, *100*, 3683. (b) Chen, J.; Vannucci, A. K.; Mebi, C. A.; Okumura, N.; Borowski, S. C.; Swenson, M.; Lockett, L. T.; Evans, D. H.; Glass, R. S.; Lichtenberger, D. L. *Organometallics* **2010**, *29*, 5330. (c) Bigi, J. P.; Hanna, T. E.; Harman, W. H.; Chang, A.; Chang, C. J. *Chem. Commun.* **2010**, *46*, 958. (d) DuBois, D. L.; Bullock, R. M. *Eur. J. Inorg. Chem.* **2011**, 1017. (e) Appel, A. M.; DuBois, D. L.; DuBois, M. R. *J. Am. Chem. Soc.* **2005**, *127*, 12717. (f) Appel, A. M.; Lee, S. J.; Franz, J. A.; DuBois, D. L.; DuBois, M. R. *J. Am. Chem. Soc.* **2009**, *131*, 5224.

(5) Shima, S.; Pilak, O.; Vogt, S.; Schick, M.; Stagni, M. S.; Meyer-Klaucke, W.; Warkentin, E.; Thauer, R. K.; Ermler, U. *Science* **2008**, *321*, 572 and references therein.

(6) (a) Wang, E. B.; Hu, C. W.; Xu, L. *Concise Polyoxometalates*, (in Chinese), 1st ed.; Chemical Industry, Beijing, 1998, 1. (b) Zheng, S. T.; Zhang, J.; Yang, G. Y. *Angew. Chem., Int. Ed.* **2008**, *47*, 3909. (c) Long, D. L.; Tsunashima, R.; Cronin, L. *Angew. Chem., Int. Ed.* **2010**, *49*, 1736. (d) Dolbecq, A.; Dumas, E.; Mayer, C. R.; Mialane, P. *Chem. Rev.* **2010**, *110*, 6009. (e) Katsoulis, D. E. *Chem. Rev.* **1998**, *98*, 359. (f) Sun, C. Y.; Liu, S. X.; Liang, D. D.; Shao, K. Z.; Ren, Y. H.; Su, Z. M. *J. Am. Chem. Soc.* **2009**, *131*, 1883.

(7) (a) Keita, B.; and Nadjo, L. Electrochemistry of Polyoxometalates. In *Encyclopedia of Electrochemistry*, Bard, A. J., Stratmann, M., Eds.; Wiley-VCH: New York, NY, 2006; Vol. 7, p 607. (b) Hill, C. L. *J. Mol. Catal. A* **2007**, *262*, 1.

(8) (a) Nohra, B.; Moll, H. E.; Albelo, L. M. R.; Mialane, P.; Marrot, J.; Draznieks, C. M.; O'Keeffe, M.; Biboum, R. N.; Lemaire, J.; Keita, B.; Nadjo, L.; Dolbecq, A. *J. Am. Chem. Soc.* **2011**, *133*, 13363. (b) Yang, L.; Kinoshita, S.; Yamada, T.; Kanda, S.; Kitagawa, H.; Tokunaga, M.; Ishimoto, T.; Ogura, T.; Nagumo, R.; Miyamoto, A.; Koyama, M. *Angew. Chem., Int. Ed.* **2010**, *49*, 5348.

(9) Koper, M. T. M.; Bouwman, E. *Angew. Chem., Int. Ed.* **2010**, *49*, 3723.

(10) (a) Xi, R.; Wang, B.; Isobe, K.; Nishioka, T.; Toriumi, K.; Ozawa, Y. *Inorg. Chem.* **1994**, *33*, 833. (b) Chen, L. D.; Wang, Y. H.; Hu, C. W.; Feng, L. Y.; Wang, E. B.; Hu, N. H.; Jia, H. Q. *J. Solid State Chem.* **2001**, *161*, 173.

(11) (a) Sheldrick, G. M. *SHELXS 97*, Program for Crystal Structure Solution; University of Göttingen: Göttingen, Germany, 1997. (b) Sheldrick, G. M. *SHELXL 97*, Program for Crystal Structure Refinement; University of Göttingen: Göttingen, Germany, 1997.

(12) (a) Zhou, Q.; Li, C. M.; Li, J.; Cui, X. Q.; Gervasio, D. *J. Phys. Chem. C* **2007**, *111*, 11216. (b) Yu, P.; Lin, Y. Q.; Xiang, L.; Su, L.; Zhang, J.; Mao, L. Q. *Langmuir* **2005**, *21*, 9000. (c) Su, B.; Hatay, I.; Trojánek, A.; Samec, Z.; Khoury, T.; Gros, C. P.; Barbe, J.; Daina, A.; Carrupt, P.; Girault, H. H. *J. Am. Chem. Soc.* **2010**, *132*, 2655. (d) Chen, H. J.; Wang, Y. L.; Dong, S. J. *Inorg. Chem.* **2007**, *46*, 10587.

(13) (a) Cheng, L.; Zhang, X. M.; Xi, X. D.; Dong, S. J . *J. Electroanal. Chem.* **1996**, *407*, 97. (b) Wang, X. L.; Qin, C.; Wang, E. B.; Su, Z. M.; Li, Y. G.; Xu, L. *Angew. Chem., Int. Ed.* **2006**, *45*, 7411. (c) Zhang, P. P.; Peng, J.; Pang, H. J.; Sha, J. Q.; Zhu, M.; Wang, D. D.; Liu, M. G. *CrystEngComm* **2011**, *13*, 3832. (d) Yang, L. F.; Kinoshita, S.; Yamada, T.; Kanda, S.; Kitagawa, H.; Tokunaga, M.; Ishimoto, T.; Ogura, T.; Nagumo, R.; Miyamoto, A.; Koyama, M. *Angew. Chem., Int. Ed.* **2010**, *49*, 5348. (e) Wang, X. L.; Hu, H. L.; Liu, G. C.; Lin, H. Y.; Tian, A. X. *Chem. Commun.* **2010**, *46*, 6485.

(14) Yang, L. F.; Kinoshita, S.; Yamada, T.; Kanda, S.; Kitagawa, H.; Tokunaga, M.; Ishimoto, T.; Ogura, T.; Nagumo, R.; Miyamoto, A.; Koyama, M. *Angew. Chem., Int. Ed.* **2010**, *49*, 5348.

(15) (a) Wang, X. L.; Li, J.; Tian, A. X.; Liu, G. C.; Gao, Q.; Lin, H. Y.; Zhao, D. *CrystEngComm* **2011**, *13*, 2194. (b) Li, Y. W.; Wang, Y. H.; Li, Y. G.; Wang, E. B. *Inorg. Chem. Commun.* **2009**, *12*, 112.

(16) (a) Kusko, A.; Dedad, J. *IEEE Ind. Appl. Mag.* **2007**, *13*, 66. (b) Reddy, R. N.; Reddy, R. G. *J. Power Sources* **2004**, *132*, 315.

(17) Zhou, Z. Y.; Chen, X. W.; Holdcroft, S. *J. Am. Chem. Soc.* **2008**, *130*, 11711.

(18) (a) Stadler, M.; Puntoriero, F.; Campagna, S.; Kyritsakas, N.; Welter, R.; Lehn, J. M. *Chem.—Eur. J.* **2005**, *11*, 3997. (b) Batema, G. D.; Lutz, M.; Spek, A. L.; Walree, C. A.; Donegá, C. M.; Meijerink, A.; Havenith, R. W. A.; Pérez-Moreno, J.; Clays, K.; Büchel, M.; Dijken, A.; Bryce, D. L.; Klink, G. P. M.; Koten, G. *Organometallics* **2008**, *27*, 1690. (c) Wang, J. H.; Fang, Y. Q.; Bourget-Merle, L.; Polson, M. I. J.; Hanan, G. S.; Juris, A.; Loiseau, F.; Campagna, S. *Chem.—Eur. J.* **2006**, *12*, 8539. (d) Ohkoshi, S.; Tokoro, H.; Hozumi, T.; Zhang, Y.;

Hashimoto, K.; Mathonière, C.; Bord, I.; Rombaut, G.; Verelst, M.; Moulin, C. C.; Villain, F. *J. Am. Chem. Soc.* **2006**, *128*, 270. (e) Censo, D. D.; Fantacci, S.; Angelis, F. D.; Klein, C.; Evans, N.; Kalyanasundaram, K.; Bolink, H. J.; Grätzel, M.; Nazeeruddin, M. K. *Inorg. Chem.* **2008**, *47*, 980.

(19) (a) Zhai, Q. G.; Lu, C. Z.; Zhang, Q. Z.; Wu, X. Y.; Xu, X. J.; Chen, S. M.; Chen, L. J. *Inorg. Chim. Acta* **2006**, *359*, 3875. (b) Luo, J. H.; Hong, M. C.; Wang, R. H.; Shi, Q.; Cao, R.; Weng, J. B.; Sun, R. Q.; Zhang, H. H. *Inorg. Chem. Commun.* **2003**, *6*, 702. (c) Wang, Y. H.; Chen, L. D.; Hu, C. W.; Wang, E. B.; Jia, H. Q.; Hu, N. H. *Chin. J. Chem.* **2002**, *20*, 22. (d) Wang, R. Z.; Xu, J. Q.; Yang, G. Y.; Bu, W. M.; Xing, Y. H.; Li, D. M.; Liu, S. Q.; Ye, L.; Fan, Y. G. *Polyhedron* **1999**, *18*, 2971. (e) Gong, Y.; Li, Y. G.; Li, H.; Wang, Y. H.; Hu, C. W. *Chin. J. Chem.* **2006**, *24*, 1148.